

The spin crossover in [Mn^{III}(pyrol)₃tren] probed by high pressure and low temperature X-ray diffraction

Philippe Guionneau^{a*}, Mathieu Marchivie^{a, b}, Yann Garcia^c, Judith A.K. Howard^d, Daniel Chasseau^a

^aInstitut de Chimie de la Matière Condensée de Bordeaux, ICMCB, UPR 9048 CNRS, Université Bordeaux I, 87 Av. dr A. Schweitzer, 33608 Pessac – France. * *e-mail*: guio@icmcb-bordeaux.cnrs.fr

^bLaboratoire de Chimie, Electrochimie Moléculaires et Chimie Analytique, UMR 6521 CNRS, Université de Bretagne Occidentale, 6 av Victor Le Gorgeu, 29238 Brest cedex 3 - France

^cUnité de Chimie des Matériaux Inorganiques et Organiques, Département de Chimie, Faculté des Sciences, Université Catholique de Louvain, Place L. Pasteur 1, 1348 Louvain-la-Neuve – Belgium.

^dChemical Crystallography Group, Chemistry Department, Durham University, South Road, Durham DH1 3LE, U.K

Abstract

The interplay between the solid state spin crossover features and the structural properties is analyzed for the [Mn^{III}(pyrol)₃tren] complex on the basis of high pressure and low temperature single crystal X-ray diffraction experiments. In particular, the low temperature (30 K, 10⁵ Pa) low spin crystal structure is compared to the low temperature (60 K, 10⁵ Pa) high spin and to the high pressure (293 K, 1.00 GPa) high spin crystal structures. The low temperature structural properties show the structural modifications due to the spin crossover in a Mn(III) complex. Comparison of these structural modifications to those described for mononuclear Fe(II) spin crossover compounds emphasizes significant differences, such as in bond lengths variation and polyhedron distortion for example. Elsewhere, analysis of the high pressure data shows that the internal stress on the metal ion is not the cause of the occurrence of the thermal spin crossover, contrary to a general belief.

PACS. 61.10.Nz X-ray diffraction 61.50.Ks Crystallographic aspects of phase transformations; pressure effects 75.30.Wx Spin-crossover 07.35.+k High pressure apparatus.

1. Introduction

The crossover from a low spin (LS) state to a high spin (HS) state presented by some transition metal compounds offers a promising example of molecular bistability for information processing. Indeed, the spin crossover (SCO) phenomenon can be driven in the solid state by a variation of temperature, by a pressure effect or by an electromagnetic radiation. The richness of this phenomenon is illustrated by the diversity of the possible features of the thermal crossover from one state to the other: abrupt (< 1 K), smooth, multi-step, full or only partial and with, or without, an hysteresis loop. This strongly interdisciplinary field is studied either for fundamental interests or potential applications and involves physicists, chemists and physical-chemists, either experimentalists or theoreticians. An impressive state of the art articles collection recently published¹ first reveals a wide view of the deep work done over the last three decades and then highlights some of the points still debated and to explore further. Among these points is the role of the application of a pressure on the SCO compounds in the solid state².

If the pressure induced SCO phenomenon has been known and theoretically studied for years it is only recently that the number of experimental magnetic studies has started to grow³. The application of pressure usually stabilizes the LS state and consequently the SCO temperature ($T_{1/2}$) increases^{4,5}. However, this statement already suffers exceptions from the few systems investigated⁶. The role of high pressure on the hysteresis width is also not clearly identified⁷. This shows that the synergy between the application of a pressure and a temperature variation on SCO compounds needs still to be understood. Since in the solid state the SCO features are closely related to the structural properties, most of the articles dedicated to high pressure magnetic data conclude to the need for high pressure structural studies.

High pressure single crystal X-ray diffraction studies of molecular compounds are still very rare, due to technical difficulties. For example, up to now (CSD search, December 2004), only 81 crystal structures determined at high pressure are reported in the Cambridge Structural Data Base which contains more than 320000 molecular crystal structures. The high pressure structural properties of only three SCO systems have been reported so far and all concern mononuclear complexes of iron(II) ions in octahedral surroundings^{8,9}.

We have investigated by single crystal X-ray diffraction the temperature and pressure dependencies of the structural properties of the mononuclear $[\text{Mn}^{\text{III}}(\text{pyrol})_3\text{tren}]$ complex which is one among the very few Mn(III) SCO systems identified^{10,11}. This compound whose crystal structure determined at room temperature revealed a $\text{Mn}^{\text{III}}\text{N}_6$ core is known to exhibit

a very abrupt spin transition from HS (5E) to LS (3T_1) around 44 K^{12, 13}. If the first goal of our study is the determination of the high pressure behavior of this compound, the investigation of the low temperature structural properties is also of great interest. First, up to now, no Mn(III) complex has been structurally characterized in both high and low spin states.. Then, recent spectroscopic measurements have evidenced the presence of a dynamic Jahn Teller distortion in the HS phase¹⁴⁻¹⁶ and questioned the role of the vibrational modes in the SCO behavior of this compound¹⁵.

To denote the crystal structure discussed thereafter we adopt the notation A-B where A corresponds to the thermodynamic conditions - HT, LT and HP for high temperature, low temperature and high pressure, respectively - and B corresponds to the spin state - HS or LS -, for example the low temperature LS crystal structure is denoted LT-LS. This study includes the determination of the isobar [293 K – 30 K] and isothermal [0 – 1.5 GPa] unit cell contractions as well as the determination of the HT-HS (293 K), LT-HS (60 K), LT-LS (30 K) and HP-HS (0.16 and 1.0GPa) crystal structures.

2. X-ray investigations details

All experiments were performed on single crystals obtained following the procedure from ref.¹⁷. Pyramidal single crystals of approximate dimensions 0.10 x 0.10 x 0.10 mm³ were used.

2.1 Low temperature investigations

The room temperature crystal structure has been re-investigated to improve the quality of the determination and to allow a rigorous comparison with subsequent experiments. The sample was mounted on a Nonius κ -CCD (MoK α) diffractometer. The unit cell volume obtained (8343 Å³) significantly differs from the one reported previously in 1981 (8377 Å³)¹². We have no explanation for such a discrepancy as a detailed analysis of the crystal structures does not show any obvious difference. However, the final quality criterion is much better in the present case (R= 2.8 %) than in the earlier published case (R= 5.9 %). Consequently these new data are used for the subsequent discussion.

Low temperature experiments were performed using an Oxford Cryosystems Helix open flow He gas cryostat combined with a Bruker SMART-CCD area detector diffractometer using the Mo K α radiation. The unit cell temperature dependence was recorded from 293 K to

30 K. Temperature cooling rate was fixed to 2 K. min⁻¹. Full data collections were run at 60 K and 30 K.

2.2 High pressure setups and measurements

Hydrostatic high pressure single crystal X-ray diffraction investigations were performed using a locally modified Diamond Anvil Cell, DAC, of the Ahsbahs type^{9,18,19} mounted on a Nonius κ -CCD (MoK α). With this kind of pressure cell, the X-ray beam goes through the gasket but not through the diamond anvil as usually for X-ray diffraction DAC. Consequently, the cell geometry offers a wide diffracting angle of about 342° rotation together with a relatively low absorption of the incident and diffracting X-ray beams. The *in situ* pressure value is measured using a deposited thin film of Nickel dimethylglyoxime known for the almost linear dependence of its light absorption properties as a function of pressure²⁰. The accuracy on the pressure value is 0.05 GPa. The pressure transmitting fluid is a FluorinertTM liquid. The cell fits perfectly on a commercial goniometer head and was mounted on a CCD diffractometer. The centering of the crystal into the X-ray beam has been performed first by centering optically the gasket and then by considering the intensity of homologous Bragg reflections.

The unit cell was determined for 14 pressure values within the range [10⁵ Pa, 1.50 GPa] using a manual search of the Bragg peaks within the collected frames. An irreversible broadening of the Bragg peaks was observed at pressure higher than 1.50 GPa.

Full data collections were run at 0.16 GPa and 1.00 GPa. Intensities were corrected from the absorption of the pressure cell pillars and the beryllium gasket using locally written programs. It is worth noting that the high pressure final structural quality criterions are of the same order of magnitude as those obtained for the ambient conditions crystal structure determination. This result appears very satisfactory in the general context of high pressure X-ray experiments. All the above structural determinations were conducted by direct methods and the refinement of atomic parameters based on full-matrix least squares on F² were performed using the SHELX-97 programs²¹ within the WINGX package²². Experimental data and results are summarized in Table 1.

TABLE 1 HERE

Figure 1 here

3 Results and discussions

3.1 Unit cell temperature dependence

The cubic symmetry of the unit cell is conserved on the whole temperature range. The unit cell undergoes a linear thermal contraction from room temperature to 45 K, then a sudden drops occurs between 45 K and 35 K (Figure 1). This very abrupt modification of the unit cell volume corresponds to the expected spin transition at ~ 44 K. The contraction of the unit cell between 45 and 35 K can therefore be attributed to the sole SCO and corresponds to a decrease of 2.0 % of the volume. This value is in perfect agreement with the commonly reported values for iron(II) SCO systems²³. Over the entire temperature range investigated, the unit cell shows a total contraction of 394 \AA^3 (4,7 %). The latter can be interpreted as the sum of the classical thermal contraction and the pure SCO effect. By subtracting the latter, the pure thermal contraction can be estimated to be 2.7 %. This value appears significantly larger than the pure thermal contraction usually observed on the same temperature range for iron(II) molecular materials²³.

3.2 Low temperature crystal structures

At room temperature, i.e. HT-HS, this compound crystallizes in the $I\bar{4}3d$ cubic space group. The manganese ion is surrounded by six nitrogen atoms and lays on a crystallographic threefold axis. The asymmetric unit therefore contains one third of the molecule. This means for example that there are only two different Mn-N bond lengths within the MnN_6 polyhedron, denoted Mn-N1 and Mn-N2 (Figure 1). These features remain unchanged whatever the temperature and the spin state, i.e. for low temperature HS and LS (Figure 2).

It is well known that the SCO corresponds to a shortening of the metal - ligand bond length. For LT-LS, the Mn-N bond lengths are significantly shorter (by 0.10 \AA) than for the LT-HS and HT-HS ones (Figure 2). This is the signature of the SCO and confirms the LS state of the complex for LT-LS. A detailed description of the temperature and pressure dependence of the MnN_6 polyhedron will be given below.

The large unit cell contraction observed in the HS state between 293 and 45 K corresponds to a crystal packing contraction. Let us in a first approach describe the crystal packing from the three shortest intermolecular Mn-Mn distances (Table 2). These distances are significantly shorter in LT-HS than in HT-HS showing that the compactness is much higher at

60 K than at 293 K. In this temperature range, these three Mn-Mn distances are shortened by almost the same amplitude (0.07 Å).

On the opposite, the re-arrangement of the crystal packing due to the SCO does not correspond to a basic contraction. Indeed, the HS to LS SCO induces on the one part a decrease of the unit cell and on the other part a reduction of the volume of each molecule due to the contraction of the MnN₆ core. The former tends to decrease the Mn-Mn distances and the latter tends to increase them. As a result of these opposite effects, . two of the Mn-Mn intermolecular distances strongly decrease and the other one slightly increases at the SCO.

Figure 2 here

Table 2 here

3.3 High pressure and occurrence of the spin crossover

The pressure dependence of the unit cell shows that the compound remains in the cubic $I\bar{4}3d$ space group on the pressure range [0 – 1.50 GPa]. A quasi linear decrease of the unit cell cubic parameter is observed within the applied pressure range (Figure 3). There is not any obvious structural transition. According to the standard deviation on pressure measurements the apparent accident at 0.5 GPa cannot be attributed to any transition, moreover a careful examination of the MnN₆ core at higher pressure clearly stand for the persistence of the HS state. The fall observed at 1.50 GPa reflects the amorphization of the sample that starts at this pressure and is effective at higher pressure as already observed for molecular materials⁹.

Figure 3 here

The Mn-N bond lengths, determined at 1.00 GPa and discussed later (Table 3) clearly show that the Mn(III) ion remains in the HS state on the whole studied pressure range. Thus no spin crossover occurs in the [0 - 1.5 GPa] pressure range at room temperature. On the one hand, this is not surprising if one considers that the spin transition temperature at ambient pressure ($T_{1/2} \sim 44$ K) is very low for this compound. Indeed, the general tendency is that the

lower $T_{1/2}$ the higher the pressure that induces the spin crossover at room temperature. Note however that some exceptions to this assumption have been already found⁶. On the other hand, in this regard, a surprising aspect is the considerable contraction of the unit cell. Indeed, from 10^5 Pa to 1.0 GPa the unit cell volume decreases by 599 \AA^3 . Let us recall that, at ambient pressure, this compound undergoes the spin transition after a thermal contraction of the unit cell from 293 K to 44 K of 222 \AA^3 and that the total contraction from 293 K to 30 K, that includes the SCO range, is 394 \AA^3 .

The occurrence of a cooperative SCO behavior can, in general, be thought in term of the internal pressure due to the neighboring molecules that stress the active ion. A complex in the LS state occupies a smaller volume than in the HS state. Consequently, as a first approximation, a strong increase of the internal pressure should induce a HS to LS crossover. In the present compound however, the unit cell pressure dependence shows that the SCO is not induced by an increase of the internal pressure on the metal ion at room temperature. Indeed, the thermal SCO starts after a unit cell thermal contraction of 2.7 % while under increasing pressure the SCO is not observed even after a unit cell contraction of 9.5 % at room temperature. The estimation from the unit cell dimensions of the volume occupied by a $[\text{Mn}^{\text{III}}(\text{pyrol})_3\text{tren}]$ molecule confirms this assumption. This volume can be estimated to be 173.8 \AA^3 at ambient conditions (HS), 169.2 \AA^3 at 60 K (HS), 165.6 \AA^3 at 30 K (LS) and only 157.3 \AA^3 at 1.40 GPa (HS).

In the literature, there are three iron(II) SCO complexes for which the high pressure crystal structures are known, $[\text{Fe}(\text{phen})_2(\text{NCS})_2]$, phen= 1,10-phenantroline⁸, $[\text{Fe}(\text{btz})_2(\text{NCS})_2]$, btz= 2,2'-bi-4,4-dihydrothiazine⁸ and $[\text{Fe}(\text{PM-TeA})_2(\text{NCS})_2] \cdot \text{CH}_3\text{OH}$, PM-Tea= N-(2'-pyridylmethylene)-4-(aminoterphenyl)aniline⁹. The first two compounds undergo a SCO at high pressure. In these two cases, the SCO induced by the low temperature or by the high pressure occurs after a very similar contraction of the HS unit cell volume. Thus, one can think in a first approximation that the occurrence of the SCO is connected to the dimension of the unit cell and thus to the internal stress on the metal ion. On the other hand, for $[\text{Fe}(\text{PM-TeA})_2(\text{NCS})_2] \cdot \text{CH}_3\text{OH}$ that undergoes a thermal but not a pressure induced SCO, the high pressure unit cell volume at 1.0 GPa is much smaller than the unit cell volume just before the thermal contraction and even much smaller than the low temperature LS unit cell volume at 10 K. Due to the presence of the inclusion of a solvent molecule within the packing, $[\text{Fe}(\text{PM-TeA})_2(\text{NCS})_2] \cdot \text{CH}_3\text{OH}$ was first considered as a particular case. However, the present study clearly evidences a similar behavior for the Mn(III) complex.

Hence, the pressure data indicates that the increase of the stress on the molecular complex, which is due to the unit cell contraction, is not a predominant factor for the occurrence of the thermal spin crossover.

3.4 Comparison of the high pressure and the low temperature crystal packing

Naturally the unit cell contraction affects the crystal packing and induces some modifications in the intermolecular contacts (Figure 4, Table 2). If the latter are considered short when they are smaller than the sum of the van der Waals radii, then the number of C...C short contacts between neighboring molecules strongly increases from ambient conditions (1 contact per ligand arm, the three arms being structurally identical) to high pressure (9 contacts per ligand arm at 1.0 GPa). Moreover, the number of short C...C contacts between neighboring complexes is the same at 30 K (LS) as at 1.0 GPa (HS). Additionally, the pressure and temperature dependencies of the geometry of the shortest C...C intermolecular contact clearly shows that the HP-HS crystal packing is closer from the LT-LS crystal packing than the HT-HS or the LT-HS ones (Table 2). This is confirmed by the modification of the corresponding intermolecular Mn...Mn distances that are similar in HP-HS and in LT-LS but significantly longer in HT-HS and LT-HS. Such C...C intermolecular contacts between the mononuclear units (Figure 4) give evidence to the origin of the cooperative effects in $[\text{Mn}^{\text{III}}(\text{pyrol})_3\text{tren}]$ and explain the occurrence of an abrupt spin transition as revealed in the magnetic measurements¹².

The meaningful decrease of the intermolecular distances perfectly reflects the strong unit cell contraction. The vicinity of the LT-LS and the HP-HS structural arrangements confirms the assumption that the internal stress is not responsible for the occurrence of the SCO in this compound. The modification with external perturbation of the whole Mn-Mn intermolecular distances shows that the HP-HS crystal packing is even more compact than the LT-LS one.

Figure 4 here

3.5 Temperature and pressure dependence of the MnN_6 polyhedron geometry

The geometry of the metal coordination sphere is in general one of the paramount factor to account for the feature of the spin crossover. First, it is now well established that the metal - ligand bond lengths are smaller and the polyhedron of coordination is less distorted in the LS state²³. Then, more interestingly, it has been recently proved in the case of iron(II) mononuclear complexes of general formula $[\text{FeL}_2(\text{NCS})_2]$ that the modification at the spin transition of the octahedrality of the $\text{Fe}^{\text{II}}\text{N}_6$ polyhedron shows a linear correlation with both the temperature of the thermal SCO and the limit temperature of the photo-induced spin crossover ($T(\text{LIESST})$)²⁵. In this case, the octahedrality was estimated from the structural parameter denoted Θ that represents the deviation of the MnN_6 geometry from a perfect octahedron (O_h) to a trigonal prismatic structure (D_{3h}); *i.e.* the trigonal deformation. The Θ parameter is calculated from the atomic coordinates and defined as the sum of the deviations from 60° of the 24 possible "twist" angles²⁵. Elsewhere, the Σ parameter defined as the sum of the deviations from 90° of the 12 cis Φ angles in the coordination sphere is another way to characterize the deviation of the polyhedron from the ideal octahedron⁹. This structural parameter has been proved to be an efficient spin state witness for the $\text{Fe}^{\text{II}}\text{N}_6$ octahedron in mononuclear complex²⁶. In order to explore such features in the case of Mn(III) complexes, it is important to report the temperature and pressure dependencies of the geometry of the $\text{Mn}^{\text{III}}\text{N}_6$ polyhedron. However, a detailed analysis of the structural - magnetic correlation at high pressure will not yet possible since there is no enough available data for Mn(III) SCO compounds. Table 3 summarizes the analysis of the MnN_6 geometry for the studied complex.

TABLE 3 HERE

First, the Mn-N bond lengths as well as the volume of the polyhedron, V_p , clearly show that the metal remains in the HS state at high pressure, at least up to 1.0 GPa. The HP-HS value of V_p does not significantly differ from the room temperature one (HS) showing that the volume of the $\text{Mn}^{\text{III}}\text{N}_6$ polyhedron depends only on the spin state and not on the thermodynamic conditions. The same result was obtained for the $\text{Fe}^{\text{II}}\text{N}_6$ octahedron. Consequently, the modification of the $\text{Mn}^{\text{III}}\text{N}_6$ polyhedron volume from 293 K to 30 K can be

attributed to the sole HS to LS crossover and thus corresponds to a decrease of 1.4 \AA^3 (12 %). This value is smaller than the modification for the $M^{II}N_6$ octahedron ($M=Co, Fe$), 3.0 \AA^3 (25 %) ¹⁸ which is not surprising as the antibonding e_g orbitals are occupied by fewer electrons in the Mn(III) case. The relatively weak modification of the MnN_6 polyhedron is also illustrated by the small differences between the HS and LS molecular structures (Figure 2).

While for Fe(II) complexes the Σ parameter increases by almost 40% from the LS to the HS states, it appears only slightly different in the LS and HS states for the $Mn^{II}N_6$ polyhedron (Table 3), with less than 10 % of variation. The obtained high pressure Σ value stands in between the HS and LS values. Moreover, the HS Θ value for the MnN_6 octahedron is of the same order of magnitude than the value for the iron complexes ²⁵. The LS Θ value appears however higher for the Mn polyhedron. The Θ value decreases with increasing pressure for the studied compound. The observed high pressure modification of the distortion, either measured with Σ or Θ , could be due to a LS conversion of a small amount of the complexes within the sample or to a pure effect of the pressure on the MnN_6 polyhedron distortion. The perfect agreement between the ambient pressure and the high pressure values of V_p , which is spin state dependents, credits however the latter assumption.

3.6 Jahn Teller effect, spin crossover and displacement parameters

It has been recently suspected from Raman studies that most of the active vibrational modes are nearly independent from the SCO for $[Mn^{III}(pyrol)_3tren]^{15}$. The displacement parameters, denoted DP, that are classically obtained from the crystal structures and reflect the vibrational modes were determined. A comparison of the temperature and pressure dependencies of the DP of the nitrogen atoms allows to shed further light on that point.

In HT-HS (293 K) the displacement parameters of the nitrogen atoms are in agreement with the usual room temperature values ($U_{eq} = 0.045 \text{ \AA}^2$). From 293 K to 60 K the DP decrease by an average value of 50 % but with a different amplitude from one nitrogen to the other. Indeed, at 60 K in LT-HS, the DP of the nitrogen atoms coordinated to the Mn atom are significantly higher (+ 30 %) than those of the other nitrogen atoms atom. Moreover, the DP of the two coordinated N atoms are also different from each other. This atypical behavior is an indication that in the temperature range where the Mn(III) remains in the HS state, [293 K – 60 K], another phenomenon involving the Mn coordination sphere occurs. Previous works based on dielectric and high frequency ESR measurements have evidenced the presence of a

dynamic Jahn Teller (JT) effect in this complex^{14,16}. The unusual DP features of the nitrogen atoms could be the signature of such effect.

From 60 K to 30 K, the DP decrease by almost 50 %. This very large drop is very unusual in this temperature range. The DP thus decrease relatively eight times more from 60 K to 30 K ($-1.7\% \text{ K}^{-1}$) than from 293 K to 60 K ($-0.2\% \text{ K}^{-1}$). This phenomenon can be clearly attributed to the SCO that occurs at $\sim 44 \text{ K}$.

Moreover, the drop of the DP from 60 K to 30 K is more pronounced for the N atoms coordinated to the Mn atom so that, at 30 K in LT-LS, the DP of all the N atoms become similar. The JT effect is weaker in LS than in HS because of the depopulation of the eg orbitals. Thus, the large modification of the DP for the N atoms probably reflects the change of the strength of the JT coupling from LS to HS. Consequently, the harmonization of the DP of the nitrogen atoms in LT-LS is in line with the presence of a dynamic JT effect in the HS state. Let us mention that a dynamical JT effect is not necessary detected from the Mn-N distances determined by XRD since the latter can correspond to average values of different Mn-N distances.

Elsewhere, when the complex is in the HS state, one of the main differences between the effect of the application of the pressure and the effect of lowering the temperature concerns in fact the displacement parameters (Figure 5). Indeed, lowering the temperature corresponds to a strong decrease of these parameters while increasing the pressure only barely affects them. In the HS state, the displacements parameters are similar at 1.0 GPa and ambient conditions. This constitutes the main difference between the HP-HS and the LT-HS crystal structures. Such remark enhances the probable role of the DP on the thermal spin crossover phenomenon.

Figure 5 here

4. Conclusions

The present investigation establishes the pressure and temperature dependencies of the structural properties and the HS and LS crystal structures of the d^4 coordination compound $[\text{Mn}^{\text{III}}(\text{pyrol})_3\text{tren}]$. It is among the few molecular SCO crystals to be characterized at high pressure. Main conclusions drawn for this complex on the basis of the present study can be summarized as follows:

i) the SCO consequences on the $\text{Mn}^{\text{III}}\text{N}_6$ polyhedron geometry are smaller than in the case of the $\text{Fe}^{\text{II}}\text{N}_6$ polyhedron. If, in general, for iron complexes the variation of the electronic entropy linked to the SCO originates in the modification of the FeN_6 polyhedron geometry, the variation of entropy due to the modification of the $\text{Mn}^{\text{III}}\text{N}_6$ polyhedron is weaker as expected from the lower electronic distribution on the t_{2g} orbitals in the Mn case. Consequently, for the Mn^{III} complex, the main origin of the variation of entropy that governs the SCO may be found elsewhere.

ii) the HS to LS SCO increases the compactness, i.e. the cooperativity, of the crystal structure that is already relatively high just before the spin crossover occurs. The HP-HS crystal structure is similar to the LT-LS one but is even more compact. C...C intermolecular contacts play a role on the cooperative behavior of the spin transition.

iii) the occurrence of the SCO is not connected to the internal stress on the metal ion in this case. This is clearly demonstrated from both the isothermal unit cell contraction and the comparison of the HP-HS, LT-HS and LT-LS crystal packing.

iiii) contrary to what was previously suspected, the vibrational modes probably play a role on the SCO phenomenon. This assumption is mainly based on both high pressure and low temperature analyses of the displacement parameters. However, this role is probably masked by the JT effect for the thermal SCO. This dynamic JT effect can be considered as a source of entropy that could play a role on the SCO occurrence for $[\text{Mn}^{\text{III}}(\text{pyrol})_3\text{tren}]$.

References

- ¹Eds. P. Gülich and H.A. Goodwin, Spin crossover in Transition Metal Compounds, Topics in Current Chemistry, Springer-Verlag Berlin Heidelberg NewYork (2004).
- ²V. Ksenofontov, A.B. Gaspar and P. Gülich, Top. Curr. Chem., **235**, 23 (2004).
- ³P. Gülich, A B Gaspar, V. Ksenofontov and Y. Garcia, J. Phys.: Condens. Matter, **16**, S1087 (2004).
- ⁴J. Jętic, R. Hinek, S.C. Capelli and A. Hauser, Inorg. Chem., **36**, 3080 (1997).
- ⁵Y. Garcia, V. Ksenofontov, G. Levchenko and P. Gülich, J. Mater. Chem., **10**, 2274 (2000).
- ⁶Y. Garcia, V. Ksenofontov, G. Levchenko, G. Schmitt and P. Gülich, J. Phys. Chem. B, **104**, 5045 (2000).
- ⁷V. Ksenofontov, G. Levchenko, H. Spiering, P. Gülich, J.F. Létard, Y. Bouhedja, O. Kahn, Chem. Phys. Lett., **294**, 545 (1998).

- ⁸T. Granier, B. Gallois, J. Gaultier, J.A. Real and J. Zarembovitch, *Inorg. Chem.*, **32**, 5305 (1993).
- ⁹P. Guionneau, C. Brigouleix, Y. Barrans, A. Goeta, J.F. Létard, J.A.K. Howard, J. Gaultier and D. Chasseau, *C. R. Acad. Sci.*, **IIc**, 161 (2001).
- ¹⁰V.V. Zelentsov and I.K. Somova, *Zh Obshch Khim*, **44**, 1309 (1974).
- ¹¹L. Kaustov, M.E. Tal, A.I. Shames and Z. Gross, *Inorg Chem*, **36**, 3503 (1997).
- ¹²Y. Garcia, O. Kahn, J.P. Ader, A. Buzdin, Y. Meurdesoif and M. Guillot, *Phys. Lett. A*, **271**, 145 (2000).
- ¹³P.G. Sim and E. Sinn, *J. Am. Chem. Soc.*, **103**, 241 (1981).
- ¹⁴M. Nakano, G. Matsubayashi and T. Matsuo, *Phys Rev B*, **66**, 212412 (2002).
- ¹⁵M. Nakano, G. Matsubayashi and T. Matsuo, *Adv Quantum Chem*, **44**, 617 (2003).
- ¹⁶S. Kimura; T. Otani, Y. Narumi, K. Kindo, M. Nakano and G. Matsubayashi, *J. Magn. Magn. Mat.*, **272-276**, 1102 (2004).
- ¹⁷P.G. Sim and E. Sinn, *Inorg. Chem.*, **17**, 1288 (1978).
- ¹⁸H. Ahsbahs, *Rev. Phys. Appl.*, **48**, 819 (1987).
- ¹⁹P. Guionneau, D. Le Pévelen, M. Marchivie, S. Pechev, J. Gaultier, Y. Barrans and D. Chasseau, *J. Phys.: Condens. Matter*, **16**, S1151 (2004).
- ²⁰J.C. Zahner and H.G. Drickamer, *J. Chem. Phys.*, **33**, 1625 (1960).
- ²¹G.M. Sheldrick, SHELXL97 and SHELXS97. release 97-2, University of Göttingen, Germany (1997).
- ²²L.J. Farrugia, *J. Appl. Cryst.*, **32**, 837 (1999).
- ²³P. Guionneau, M. Marchivie, G. Bravic, J.F. Létard and D. Chasseau, *Top. Curr. Chem.*, **234**, 97 (2004).
- ²⁴M. Marchivie, P. Guionneau, J.F. Létard and D. Chasseau, *Acta Cryst.*, **B61**, 25 (2005).
- ²⁵P. Guionneau, M. Marchivie, G. Bravic, J.F. Létard and D. Chasseau, *J. Mater. Chem.*, **12**, 2546 (2002).

Acknowledgements

We thank the ALLIANCE program for a bilateral grant between the Durham and the Bordeaux groups and the Fonds Special de Recherche of the University of Louvain for financial help.

Table 1. Summary of single crystal X-ray diffraction data for $[\text{Mn}^{\text{III}}(\text{pyrol})_3\text{tren}]$. Crystallographic details including atomic parameters in cif format have been deposited with the Cambridge Crystallographic data Centre with number CCDC 266992-266996.

| Formula | $\text{C}_{21}\text{H}_{24}\text{N}_7\text{Mn}$ | | | | |
|--|---|--------------|--------------|--------------|--------------|
| Crystal morphology | 0.10 x 0.10 x 0.10 mm ³ , pyramidal | | | | |
| T(K) | 293(2) | 60(5) | 30(5) | 293(2) | 293(2) |
| applied P (GPa) | 0 | 0 | 0 | 0.16(5) | 1.00(5) |
| Crystal syst. | cubic | | | | |
| Space group | $\bar{I}43d$ | | | | |
| Z-space group | 48 | | | | |
| Z-formula | 16 | | | | |
| a(Å) | 20.282(5) | 20.101(4) | 19.958(1) | 20.215(4) | 19.784(1) |
| V(Å ³) | 8343(6) | 8121(1) | 7949(1) | 8261(5) | 7744(1) |
| Density(calc.) | 1.367 | 1.405 | 1.435 | 1.381 | 1.473 |
| μ mm ⁻¹ | 0.66 | 0.67 | 0.69 | 0.66 | 0.71 |
| $\theta_{\text{min/max}}$ (°) | 2.5 / 25.0 | 3.2 / 27.4 | 3.2 / 27.4 | 6.2 / 20.8 | 2.5 / 21.9 |
| Collected refl. | 26617 | 17855 | 20992 | 10445 | 10558 |
| Indep. refl. | 1234 | 1513 | 1488 | 359 | 407 |
| Rint | 0.05 | 0.06 | 0.06 | 0.11 | 0.06 |
| Obs. refl. ($I/\sigma(I)=2$) | 1106 | 1410 | 1430 | 217 | 227 |
| Nb. parameter | 88 | 88 | 88 | 88 | 88 |
| R_{obs} | 0.028 | 0.033 | 0.033 | 0.046 | 0.039 |
| R_{all} | 0.039 | 0.038 | 0.035 | 0.114 | 0.112 |
| $wR2_{\text{obs}}$ | 0.067 | 0.076 | 0.078 | 0.108 | 0.086 |
| $\Delta\rho_{\text{max}}/\Delta\rho_{\text{min}}$ (e-Å ⁻³) | 0.60 / -0.97 | 0.21 / -0.29 | 0.34 / -0.39 | 0.17 / -0.15 | 0.27 / -0.16 |

Table 2. Distances (Å) and angles (°) corresponding to the shortest C...H-C intermolecular contact within the crystal packing of [Mn^{III}(pyrol)₃tren]. Modifications with increasing pressure and lowering the temperature of the geometric parameters for this intermolecular contact and the corresponding Mn...Mn distance. For symmetrical reasons this contact appears three times for a same molecule (Figure 4) and concerns the following symmetry operators: (1/2-x, y, -z), (-x, 1/2-y, z) and (x, -y, 1/2-z). The two other shortest Mn...Mn intermolecular distances between neighboring complexes are also given.

| | 293 K | 60 K | 30 K | 1.0 GPa |
|--|----------|----------|----------|-----------|
| <i>notation</i> | HT-HS | LT-HS | LT-LS | HP-HS |
| <i>shortest intermolecular C...H-C</i> | | | | |
| C...C | 3.473(4) | 3.415 | 3.387(3) | 3.32(1) |
| C...H-C | 2.96 | 2.91 | 2.93 | 2.8 |
| (C...H-C) angle | 114.0(1) | 112.6(1) | 110.0(1) | 112(1) |
| Mn...Mn | 7.589(4) | 7.511(3) | 7.391(3) | 7.401(15) |
| <i>Other Mn ... Mn distances, between Mn(x, y, z) and Mn (given symmetry operation)</i> | | | | |
| (y, z, x) | 8.782(4) | 8.704(3) | 8.642(3) | 8.568(15) |
| (-y, 1/2-z, x) | 9.955(4) | 9.881(3) | 9.914(3) | 9.714(15) |

Table 3. Geometric parameters of the $\text{Mn}^{\text{III}}\text{N}_6$ polyhedron as a function of temperature and pressure: Mn-N distances, d , and distortion angles Σ that is the sum of the deviations from 90° of the 12 cis Φ angles in the coordination sphere [9] and Θ that is defined as the sum of the deviations from 60° of the 24 possible "twist" angles [14]. V_p is the volume of the MnN_6 octahedron [24].

| | 293 K | 60 K | 30 K | 0.16 GPa | 1.0 GPa |
|-------------------------|----------|----------|----------|-----------|----------|
| spin state | HS | HS | LS | HS | HS |
| $d_{\text{Mn-N1}}$ (Å) | 2.052(2) | 2.054(2) | 1.975(2) | 2.054(10) | 2.046(8) |
| $d_{\text{Mn-N2}}$ (Å) | 2.127(2) | 2.125(2) | 2.027(2) | 2.130(10) | 2.110(8) |
| Σ ($^\circ$) | 71(1) | 71(1) | 64(1) | 71(5) | 67(4) |
| Θ ($^\circ$) | 240 | 239 | 199 | 230 | 222 |
| V_p (Å ³) | 11.8(1) | 11.8(1) | 10.4(1) | 11.7(5) | 11.7(5) |

Figure 1. Temperature dependence of the cubic unit cell parameter of $[\text{Mn}^{\text{III}}(\text{pyrol})_3\text{tren}]$ in the range [293 K – 30 K] and scheme of the complex with N atom labels(inset).

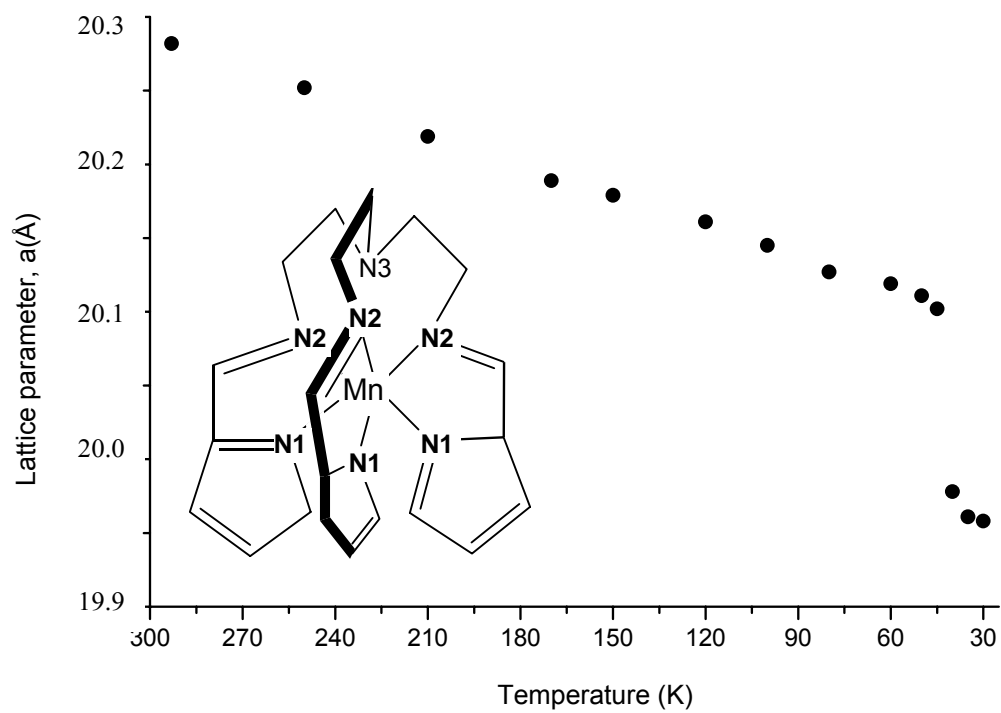
Figure 2. View of the $[\text{Mn}^{\text{III}}(\text{pyrol})_3\text{tren}]$ complex in the HS state at 60 K, LT-HS, (black) and at in the LS state at 30 K, LT-LS, (Gray). The two Manganese atoms have been superimposed for comparison showing the relatively small shortening and the weak distortion induced by the SCO.

Figure 3. Pressure dependence of the cubic unit cell parameter of $[\text{Mn}^{\text{III}}(\text{pyrol})_3\text{tren}]$. Pressure value accuracy is ± 0.05 GPa. Amorphization takes place at around 1.50 GPa.

Figure 4. view of a $[\text{Mn}^{\text{III}}(\text{pyrol})_3\text{tren}]$ complex along its three fold axis together with the three corresponding symmetry generated neighbouring complexes. The shortest C...H-C intermolecular contact is represented by dots. Symmetry operations: $(1/2-x, y, -z)$, $(-x, 1/2-y, z)$ and $(x, -y, 1/2-z)$.

Figure 5. Atomic displacement ellipsoids (80% probability) in $[\text{Mn}^{\text{III}}(\text{pyrol})_3\text{tren}]$ for the different experimental (P, T) conditions.

Figure 1. Temperature dependence of the cubic unit cell parameter of $[\text{Mn}^{\text{III}}(\text{pyrol})_3\text{tren}]$ in the range [293 K – 30 K] and scheme of the complex with N atom labels(inset)



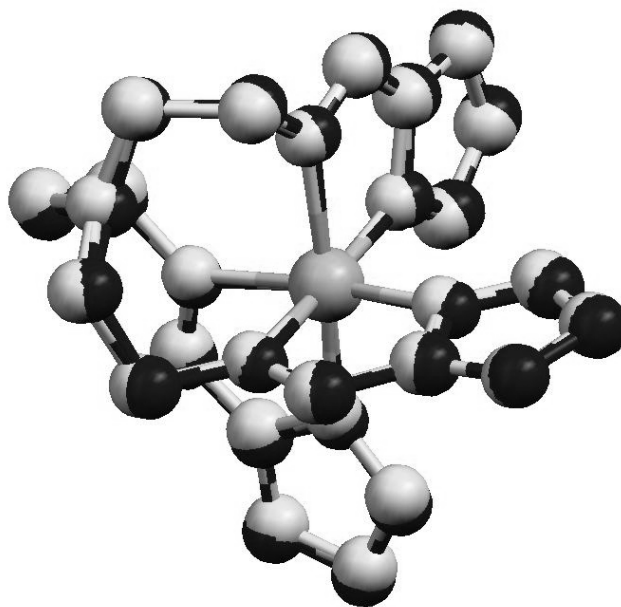
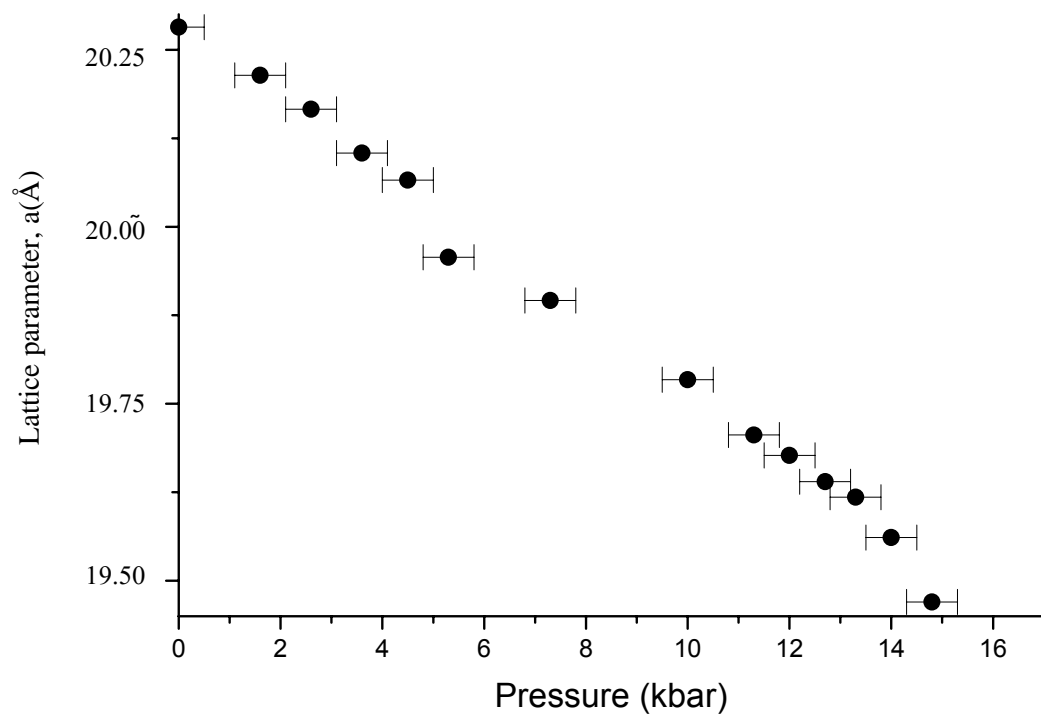


Figure 2. View of the [Mn^{III}(pyrol)₃tren] complex in the HS state at 60 K, LT-HS, (black) and at in the LS state at 30 K, LT-LS, (Gray). The two Manganese atoms have been superimposed for comparison showing the relatively small shortening and the weak distortion induced by the SCO.

Figure 3. Pressure dependence of the cubic unit cell parameter of $[\text{Mn}^{\text{III}}(\text{pyrol})_3\text{tren}]$. Pressure value accuracy is ± 0.05 GPa. Amorphization takes place at around 1.50 GPa.



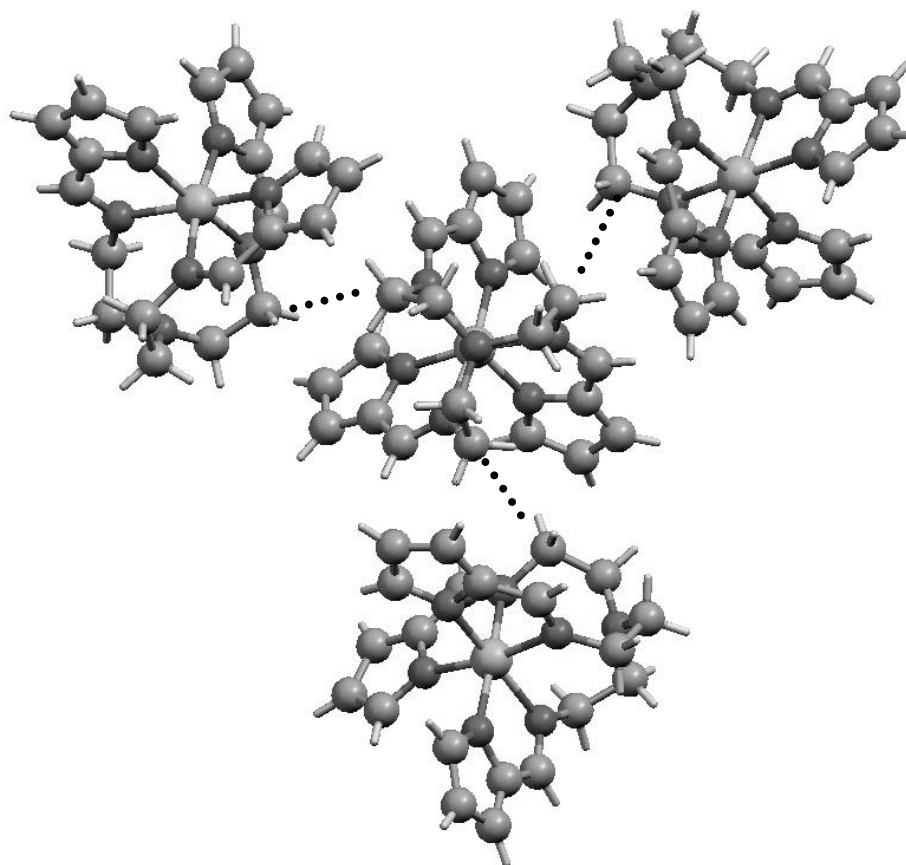


Figure 4. view of a [Mn^{III}(pyrol)₃tren] complex along its three fold axis together with the three corresponding symmetry generated neighboring complexes. The shortest C...H-C intermolecular contact is represented by dots. Symmetry operations: $(1/2-x, y, -z)$, $(-x, 1/2-y, z)$ and $(x, -y, 1/2-z)$.

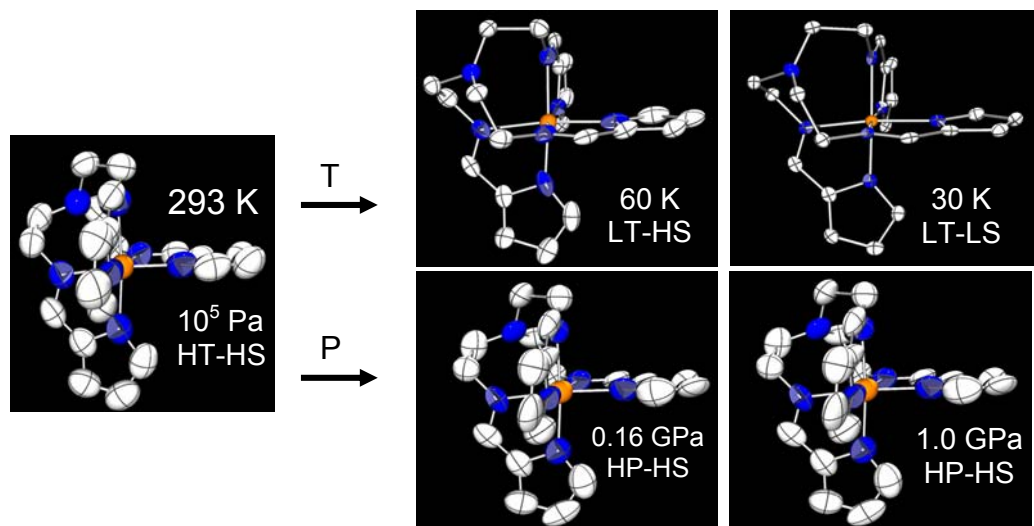


Figure 5. Atomic displacement ellipsoids (80% probability) in $[\text{Mn}^{\text{III}}(\text{pyrol})_3\text{tren}]$ for the different experimental (P, T) conditions.